Citation
Yuan, C. and Chen, W. and Pham, T.M. and Hao, H. and Cui, J. and Shi, Y. 2020. Interfacial bond behaviour between hybrid carbon/basalt fibre composites and concrete under dynamic loading. International Journal of Adhesion and Adhesives. 99: ARTN 102569. http://doi.org/10.1016/j.ijadhadh.2020.102569

Interfacial Bond Behaviour between Hybrid Carbon/Basalt Fibre Composites and Concrete under Dynamic Loading

Cheng Yuan[1], Wensu Chen[1*], Thong M. Pham[1], Hong Hao[1]*, Cui Jian[2], Yanchao Shi[2]

[1]Centre for Infrastructural Monitoring and Protection, School of Civil and Mechanical Engineering, Curtin University, Australia
[2]Tianjin University and Curtin University Joint Research Center of Structure Monitoring and Protection, School of Civil Engineering, Tianjin University, China
**Corresponding Authors*

Abstract

An experimental investigation on the dynamic interfacial bond behaviours between hybrid carbon/basalt fibre reinforced polymer (FRP) sheets and concrete under high loading velocities (i.e., 8.33E-6, 1.0, 3.0, and 8.0 m/s) is carried out in this study. The single-lap shear specimens are evaluated with different stacking sequences of FRP sheets (i.e., CFRP and BFRP) bonded to the concrete substrates. Experimental results including debonding failure modes, ultimate debonding strain, debonding load, interfacial fracture energy, and bond-slip response are discussed and evaluated. The testing results show that the interfacial bond behaviours between either sole FRP sheet or hybrid carbon/basalt FRP composite and concrete are sensitive to strain rate. The sole FRP sheet exhibits higher strain rate sensitivity than hybrid composite. The interfacial shear resistance between hybrid FRP sheets and concrete is improved due to the effect of FRP hybridization and strain rate. Additionally, the stacking sequence of FRP composites results in different bond performance when the loading speed is less than 1 m/s, while the effect of stacking sequence on bonding behaviour is insignificant when the loading speed is over 1 m/s. The hybrid composites have a relatively longer effective bond length under both quasi-static and dynamic loadings. Empirical formulae are proposed based on the test data to predict the dynamic interfacial bonding strength and shear stress between single or hybrid FRP sheet and concrete at various strain rates.

Keywords: Strain rate; Dynamic interfacial bond behaviour; Hybrid FRP composites; Single-lap shear tests.

1. Introduction

Natural or man-made hazards such as earthquakes, collisions, explosions, etc., may cause structural damage and economic loss. To strengthen reinforced concrete (RC) structures against these hazards, various strengthening techniques have been applied. Fibre-reinforced polymer (FRP), as an effective strengthening composite material with high strength to weight ratio and great corrosion resistance, has been widely used to strengthen RC structures [1, 2]. Premature FRP debonding failure has detrimental effects on the strengthening performance and consequently only around 40% of the FRP strength can be utilized [3]. To better unveil the mechanism of FRP debonding, numerous studies have been implemented to examine the interfacial bond performance. The corresponding interfacial bond-slip models have been proposed to evaluate the debonding behaviours [4].

To suppress the premature FRP debonding, various techniques such as anchorage systems and hybrid FRP composites have been used [5]. Among these methods, using hybrid FRP composites, consisting of different types of FRP, can take advantage of the superiority of each type of fibre. The fibres with lower rupture strain fractures prior to the fibres with higher rupture strain, which can be used as a warning sign before reaching the ultimate failure of the hybrid FRP composite [6]. In addition, the ultimate rupture strain of the hybrid FRP composites can be improved by the hybrid effect [7]. Naik et al. [8] found that the impact resistance capacity was enhanced by using hybrid composites (glass-carbon/epoxy) through experimental studies. Ribeiro et al. [9] experimentally examined the tensile properties of hybrid FRP composites (CFRP/GFRP and CFRP/BFRP) and reported their good pseudo-ductile tensile behaviour.

Meanwhile, hybrid FRP composites have been used to strengthen RC beams in the previous studies. Kim and Shin [10] carried out an experimental study and observed the significant influence of FRP stacking sequence on the load-bearing capacity and the ductility of RC beam strengthened by hybrid carbon and glass fibres . Concrete crushing was observed before the FRP composites reached its failure. Li et al. [11] reported that hybrid composite consisting of CFRP and GFRP sheets is more effective in strengthening as compared to sole FRP sheets. Choi et al. [12] reported that the RC beams strengthened with stiffer and thinner CFRP sheets had higher load-carrying capacity while those RC beams strengthened with hybrid FRPs showed higher ductility by carrying out experimental and analytical studies. Yuan et al. [13] experimentally examined the bond performance between hybrid composites and concrete and found that the stacking sequence of the composite remarkably influences the bond-slip response. Increasing FRP layers might result in relative slippage between FRP layers and consequently resulted in a relatively higher shear slip.

FRP-strengthened RC beams may be subjected to dynamic loads such as impact and blast [14, 15]. Kadioglu and Adams [16] reported that the behaviour of tape under impact shear was different from that under quasi-static. Therefore, it is essential to investigate the dynamic bond performance of the FRP-to-concrete interface. Currently, very limited experimental investigations have been carried out on the dynamic interfacial bond behaviour of FRP-concrete interface in the literature. Yuan et al. [17] experimentally tested the BFRP-to-SFRC under high strain rate by considering the effect of volume of steel fibres on the interfacial bond behaviour and found that the BFRP-to-SFRC interface was strain rate dependent. Huo et al. [18] conducted tests on GFRP-strengthened RC beams to indirectly examine the bonding behaviour with the strain rate up to 5 s^{-1}. It was reported that the shear resistance increased significantly with the rising loading rate. Salimian et al. [19] carried out an experimental study on the effect of loading rate on the interfacial bond between CFRP and concrete. The maximum loading rate of 60 mm/min was used to conduct the single-lap shear tests. Single-lap shear test has been widely used to study the behaviour of adhesive joints [16, 20]. It should be noted that the existing studies on the dynamic interfacial bond behaviour only cover the strain rate up to 5 s^{-1}. In addition, no study has been carried out on the dynamic interfacial bond performance between hybrid composites and concrete.

In this study, single-lap shear tests were carried out to examine the effect of strain rate ranging from 2.50E-5 to 155.10 s^{-1} on the interfacial bond behaviours between hybrid FRP composites and concrete. The hybrid composites consist of one layer of CFRP sheet with a relatively high tensile strength and one layer of BFRP sheet with relatively high rupture strain. The evaluation and discussion regarding the failure mode, strain distributions, interfacial fracture energy, and bond-slip response were reported in this study.

2. Experimental program

2.1 Material properties

The single-lap shear tests were carried out to study the dynamic interfacial bond properties between hybrid composites and concrete. Forty-four FRP-to-concrete specimens were prepared in total. The concrete substrate had 30.14 MPa compressive strength and 3.12 MPa tensile strength. The dimension of the concrete block was 150 mm x 150 mm x 300 mm, and the dimension of the carbon fibre (CFRP), basalt fibre (BFRP), and hybrid composites (HCB) were 40 mm x 400 mm. The nominal thickness of the CFRP and BFRP sheet was 0.167 mm and 0.12 mm, respectively. The bond area was 40 mm x 200 mm with a 50 mm unbonded region reserved at the loaded end to eliminate the concrete edge effect. Details of the specimens are shown in Figure 1. The specimen with stacking order of 1C1B denotes one non-attaching layer of CFRP (1C) and one attaching layer of BFRP (1B) to concrete substrate, as shown in Figure 1. The measured mechanical properties of FRPs (CFRP, BFRP, and HCB) were summarized in Table 1.

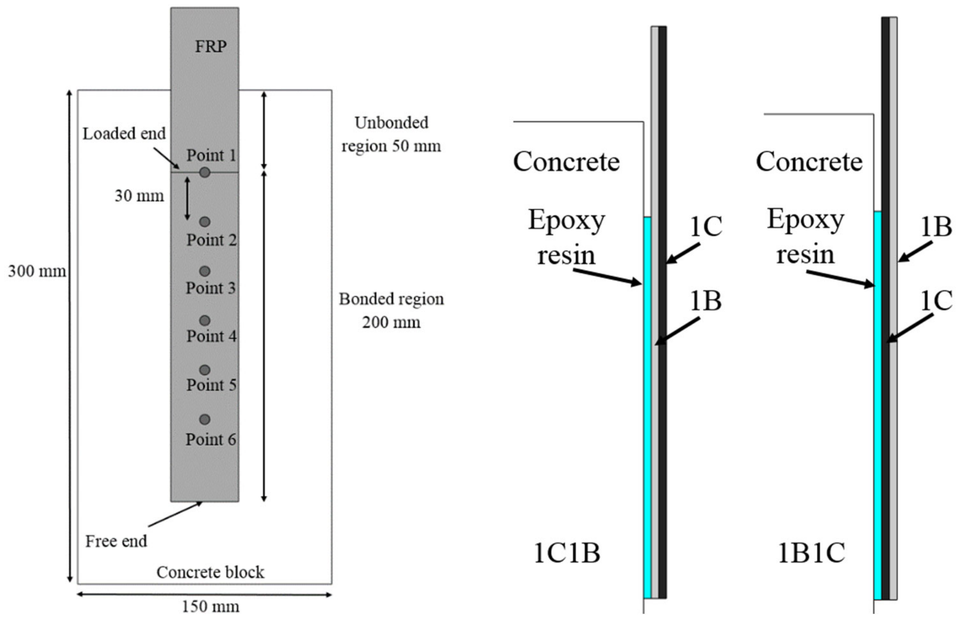

Figure 1. Specimen details (L) and stacking sequence of FRP sheets (R)

Table 1. Mechanical properties of FRP sheets

Material	Elastic modulus (GPa)	Rupture strain (%)	Tensile strength (MPa)	Nominal thickness (mm)	Stiffness $E_f t_f$ (N/mm)
CFRP (1C)	210	1.21	2450	0.167	35.07
BFRP (1B)	73	1.85	1400	0.120	8.76
1C1B/1B1C	147	1.36	2050	0.287	42.20

2.2 Test setup

Figure 2 (a) illustrates the testing machine (INSTRON@ VHS 160-20) used in this study, which can generate a constant loading velocity from 0.1 m/s to 25 m/s. The designed loading speed can be realized by the fast jaw and the acceleration is measured by an accelerometer which was mounted on the fast jaw. To avoid any in-plane and out-of-plane movement, the designed holding frame was used to hold the specimen in place as shown in Figure 2 (b). The dynamic debonding process was recorded by a high-speed camera and the obtained successive digital images were used to conduct the Digital Image Correlation (DIC) analysis, as shown in Figure 2 (c, d). Specimen surface was prepared with white base and black speckle pattern.

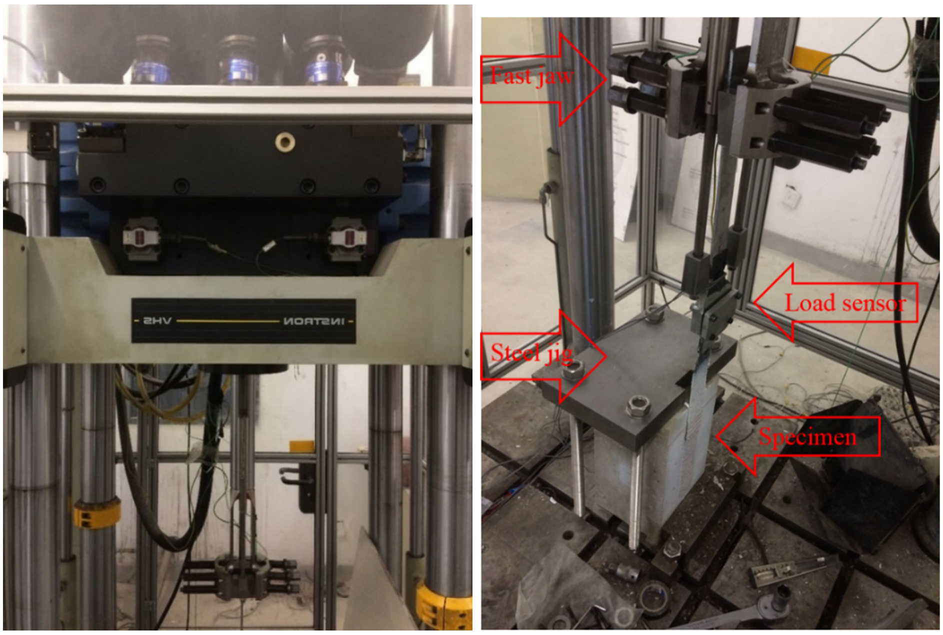

(a) Testing machine (b) Test setup

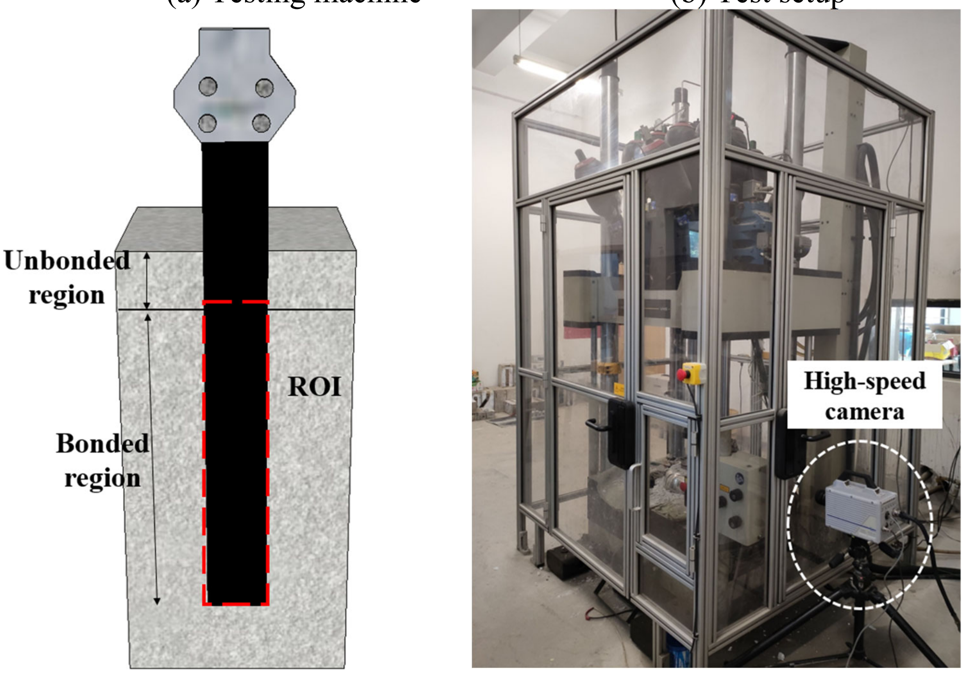

(c) Region of interest; (d) High-speed camera

Figure 2. Test facility and setup

3. Experimental results and discussions

Dynamic single-lap shear testing results are valid only when the dynamic stress equilibrium is achieved. Therefore, validation of stress equilibrium is conducted first, the details are presented in Section 3.2 by comparing the FRP surface strain derived from the DIC technique. The measurement accuracy was verified by matching the readings from strain gauges and those from the DIC technique. The technique has been well applied in the previous study [21].

3.1 Failure mode and bond strength

Under dynamic loadings, some debris consisting of mortar and coarse aggregates were stripped off with the detachment of FRP sheet, indicating that the dynamic debonding process should release greater fracture energy. The typical failure modes after testing are shown in Figure 3. After the detachment of FRP sheets, a flake layer of concrete beneath the FRP was observed under quasi-static loading, indicating that the shear stress penetrated the weakest part of the concrete layer. Since there was no normal stress applied in the single-lap shear test, shear stress changed into tensile stress along 45^{o} plane and consequently fracture initiated on the tensile side of concrete substrate [22]. However, with the increased loading rate, a combined failure was observed as the debonding location was shifted from concrete to concrete-epoxy interface. The changed pattern of the debonding mode indicates that the interfacial shear resistance of FRP-concrete interface was enhanced with strain rate, which was caused by the improved concrete tensile strength. When subjected to a relatively low loading rate, the microcracks initiate and propagate along the interfacial transition zone (ITZ) since it is the weakest part in strength as compared to aggregates and mortar. However, there is not enough time for the cracks to initiate and propagate along the weakest part due to the short loading duration under high loading rates. Therefore, the debonding interface shifted from the enhanced concrete layer to the concrete-epoxy interface with the rising strain rate. Fracture of adhesive can be observed in some cases with the strain rate over 30 s^{-1}. As the adhesive has a stronger tensile strength than concrete, fracture in the adhesive layer resulted in higher debonding load. Additionally, the hybrid composites (i.e., 1C1B or 1B1C) showed similar debonding failure modes as the sole composite (i.e., 1C or 1B). Similar observation is also reported in a previous study [13]. For easier presentation, notations are introduced to denote quasi-static and dynamic tests. The specimen identification "*QSCB-m*" refers to the quasi-static test of 1C1B, and *m* represents the specimen number. The specimen identification "*DCB-n-m*" represents the dynamic test of 1C1B, the letter *n* represents the loading speed, and the letter *m* represents the specimen number.

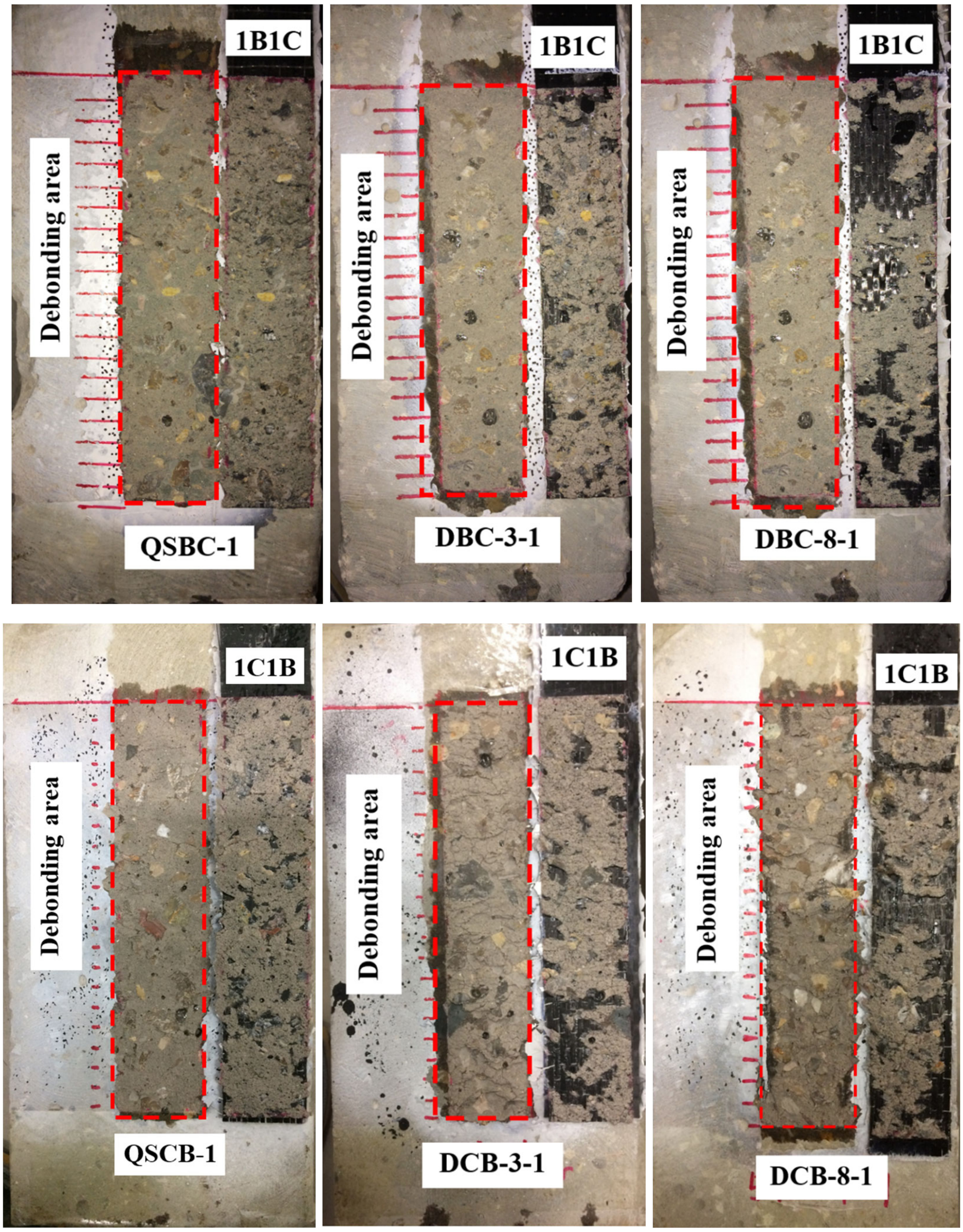

Figure 3. Typical failure modes of specimens from quasi-static and dynamic tests

Table 2. Test results

Specimen ID	FRP	FRP stiffness (N/mm)	Loading velocity (m/s)	Strain rate (s^{-1})	***Pu*** **(kN)**	ε_u **(%)**	τ_m **(MPa)**	s_o **(mm)**	G_f **(N/mm)**	$f_{t.DIF}$ **(MPa)**	***A*** **(mm)**	***B*** **(mm)**	Failure mode
QSC-1	CFRP	35.07	8.33E-6	2.50E-5	9.31	0.664	3.98	0.98	0.77	2.89	10.81	16.09	C
QSC-2	CFRP	35.07	8.33E-6	2.50E-5	8.99	0.641	3.92	0.94	0.72	2.89	10.64	16.28	C
QSB-1	BFRP	8.76	8.33E-6	2.50E-5	3.98	1.136	2.04	1.34	0.57	2.89	6.56	6.61	C
QSB-2	BFRP	8.76	8.33E-6	2.50E-5	3.73	1.064	1.98	1.24	0.50	2.89	6.72	6.43	C
QSCB-1	1C1B	42.20	8.33E-6	2.50E-5	10.52	0.663	4.71	1.35	0.93	2.89	7.11	13.49	C
QSCB-2	1C1B	42.20	8.33E-6	2.50E-5	10.58	0.651	4.89	1.41	0.89	2.89	7.49	12.98	C
QSBC-1	1B1C	42.20	8.33E-6	2.50E-5	10.98	0.613	4.51	1.25	0.79	2.89	7.94	11.97	C
QSBC-2	1B1C	42.20	8.33E-6	2.50E-5	11.09	0.639	4.72	1.19	0.86	2.89	7.89	12.45	C
DC-1-1	CFRP	35.07	1.0	14.98	11.31	0.806	6.49	1.02	1.14	5.06	9.57	11.13	C
DC-1-2	CFRP	35.07	1.0	20.03	10.86	0.774	6.57	0.92	1.05	5.11	9.74	12.01	C
DC-1-3	CFRP	35.07	1.0	19.75	11.29	0.805	6.41	0.94	1.14	5.11	10.38	11.37	C
DC-3-1	CFRP	35.07	3.0	49.75	13.05	0.930	7.25	1.05	1.52	6.19	11.18	9.31	C/CE
DC-3-2	CFRP	35.07	3.0	47.20	13.31	0.949	7.84	1.10	1.58	6.08	10.78	9.12	C/CE
DC-3-3	CFRP	35.07	3.0	39.90	13.59	0.969	7.63	1.07	1.65	5.75	11.22	9.26	C
DC-8-1	CFRP	35.07	8.0	116.33	14.31	1.020	11.31	0.96	1.82	8.21	11.87	11.19	C/CE
DC-8-2	CFRP	35.07	8.0	126.36	13.95	0.994	11.19	0.94	1.73	8.44	10.97	12.36	C/CE
DC-8-3	CFRP	35.07	8.0	127.97	14.90	1.062	12.04	1.04	1.98	8.48	10.78	13.02	C/CE
DB-1-1	BFRP	8.76	1.0	25.80	4.09	1.167	4.11	1.21	0.60	5.16	16.60	11.79	C
DB-1-2	BFRP	8.76	1.0	33.20	5.43	1.550	4.26	1.23	1.05	5.21	10.66	7.70	C
DB-1-3	BFRP	8.76	1.0	29.40	4.62	1.318	4.09	1.18	0.76	5.18	10.12	9.81	C
DB-3-1	BFRP	8.76	3.0	46.60	6.28	1.792	5.12	1.20	1.41	6.05	19.89	11.20	C/CE
DB-3-2	BFRP	8.76	3.0	53.50	5.74	1.638	4.79	1.17	1.18	6.34	20.88	12.18	C/CE
DB-3-3	BFRP	8.76	3.0	54.30	5.17	1.475	5.56	1.15	0.95	6.37	18.21	10.09	C/CE
DB-8-1	BFRP	8.76	8.0	155.10	7.23	1.918	6.56	1.06	1.61	9.04	14.35	8.61	C/CE
DB-8-2	BFRP	8.76	8.0	150.10	7.02	2.003	6.29	1.13	1.76	8.94	19.98	13.12	C/CE
DB-8-3	BFRP	8.76	8.0	130.40	6.80	1.852	6.82	1.09	1.50	8.53	21.12	13.67	C/CE
DCB-1-1	1C1B	42.20	1.0	16.89	13.03	0.772	5.78	1.21	1.26	5.08	8.63	11.25	C
DCB-1-2	1C1B	42.20	1.0	12.40	12.93	0.766	5.92	1.18	1.24	5.02	8.72	11.92	C
DCB-1-3	1C1B	42.20	1.0	13.66	12.33	0.731	6.02	1.14	1.13	5.04	9.32	14.11	C
DCB-3-1	1C1B	42.20	3.0	46.96	14.08	0.834	8.08	1.16	1.47	6.07	7.64	9.58	C/CE
DCB-3-2	1C1B	42.20	3.0	50.26	14.89	0.882	7.79	1.09	1.64	6.21	8.78	11.05	C/CE
DCB-3-3	1C1B	42.20	3.0	39.46	14.35	0.850	7.67	1.03	1.52	5.73	9.11	10.54	C/CE
DCB-8-1	1C1B	42.20	8.0	98.21	17.55	1.006	11.10	1.04	2.13	7.76	15.23	14.24	C/CE
DCB-8-2	1C1B	42.20	8.0	95.95	17.08	0.928	11.89	1.01	1.82	7.70	16.21	12.49	C/CE
DCB-8-2	1C1B	42.20	8.0	87.46	16.81	0.996	12.08	1.05	2.09	7.47	17.19	13.24	C/CE
DBC-1-1	1B1C	42.20	1.0	14.37	11.97	0.709	6.69	1.19	1.06	5.05	10.98	17.21	C
DBC-1-2	1B1C	42.20	1.0	15.12	13.22	0.783	7.51	1.11	1.29	5.06	12.99	16.19	C
DBC-1-3	1B1C	42.20	1.0	14.68	13.25	0.785	6.34	1.09	1.30	5.05	12.96	15.64	C
DBC-3-1	1B1C	42.20	3.0	44.54	14.74	0.873	8.18	1.11	1.61	5.96	13.51	13.49	C
DBC-3-2	1B1C	42.20	3.0	50.58	13.99	0.829	9.16	1.06	1.45	6.22	14.13	12.76	C/CE
DBC-3-3	1B1C	42.20	3.0	44.95	15.17	0.899	8.79	1.12	1.70	5.98	15.12	11.29	C/CE
DBC-8-1	1B1C	42.20	8.0	114.11	17.66	1.004	11.57	1.02	2.13	8.16	14.92	15.26	C/CE
DBC-8-2	1B1C	42.20	8.0	107.85	17.07	1.012	12.13	1.11	2.16	8.01	15.38	14.68	C/CE
DBC-8-3	1B1C	42.20	8.0	118.96	16.91	0.942	11.95	1.03	1.87	8.27	17.11	11.47	C/CE

Note: *C* means the fracture of concrete layer; *CE* means the debonding initiated from the concrete-to-epoxy interface.

Figure 4 illustrates the typical load-slip curves corresponding to different loading velocities. In general, the debonding load and the shear slip raised significantly with the rising strain rate for all the tested specimens, indicating that the debonding plateau under dynamic loading is longer than the case under quasi-static loading. According to the previous study, the load-slip curves can be separated into three regions during the debonding process [23], as shown in Figure 5. Region one refers to the linear-elastic stage, where the interfacial bond experiences minor shear slips with the high interfacial stiffness. Region two is the softening stage caused by microcracks of concrete, where the interfacial bond stiffness decreases with large shear slips. Region three is the debonding stage, where the bond deteriorates with increasing slips till the final debonding of FRP sheets. Irrespective of the quasi-static or dynamic loading condition, both the sole FRP sheets and hybrid composites exhibited three regions in the load-slip curves, indicating that hybrid composite has no effect on load and slip response mode.

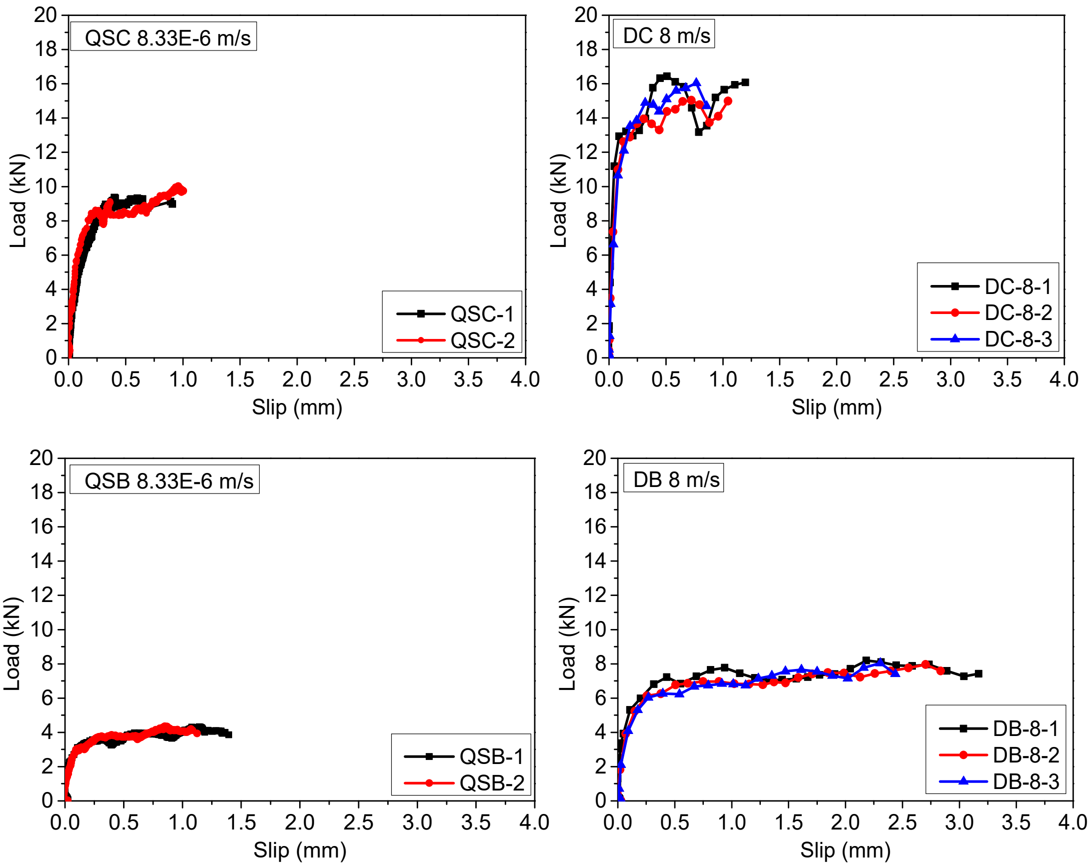

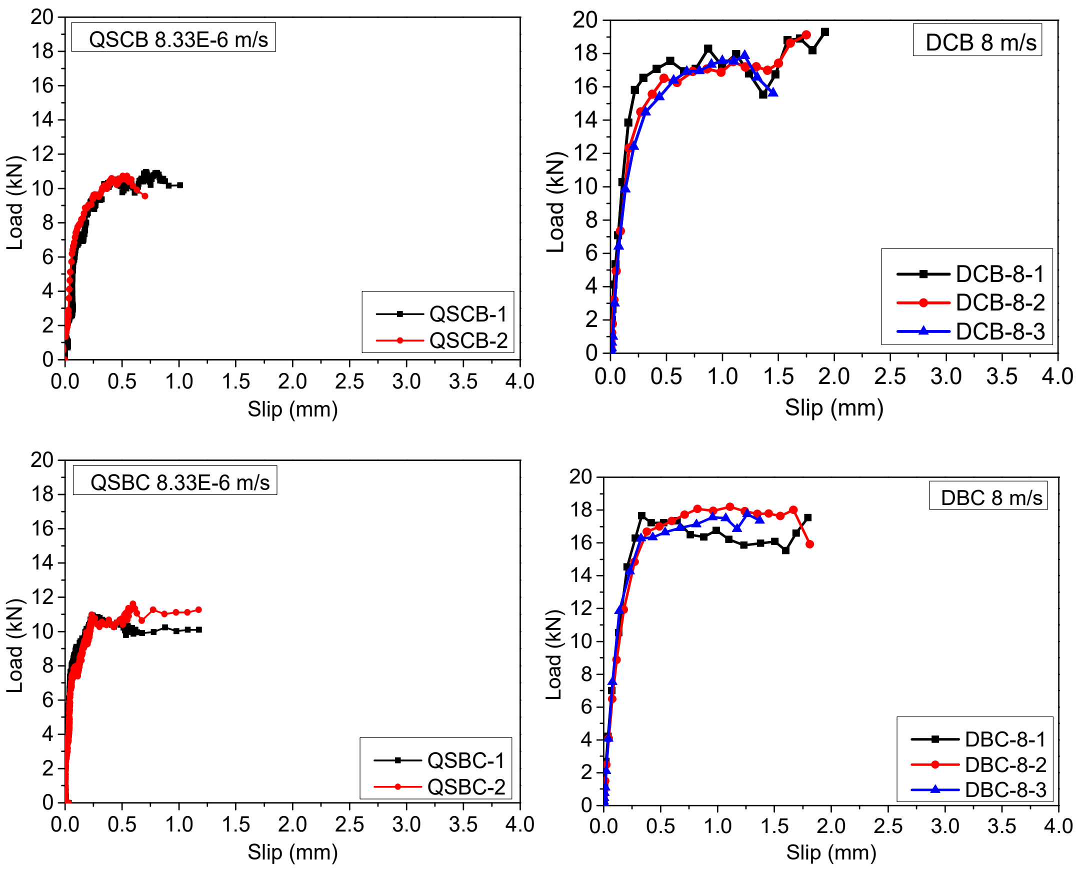

Figure 4. Load-slip responses

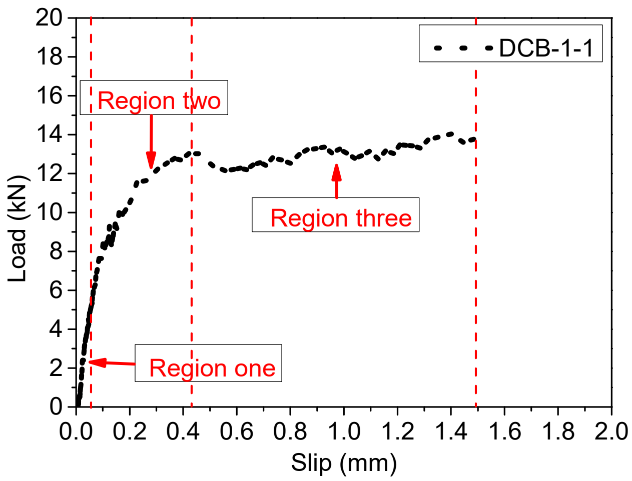

Figure 5. Three regions of a typical bond-slip curve

Figure 6 compares the average debonding load of all the tested specimens. The increment of debonding load and shear slip indicates that the bonding behaviour of FRP-concrete interface is strain rate dependent. These observations agree well with findings from the previous study [18]. As compared with the specimen of 1B-concrete interface, the 1C-concrete interface showed a relatively higher debonding load at each loading rate due to the greater stiffness of CFRP plate. However, the debonding process of the specimen 1B-concrete was more ductile than 1C-concrete with higher shear slip at the loaded end. Given the same FRP stiffness but different FRP stacking sequence, the debonding load of specimen 1B1C-concrete was higher than that of specimen 1C1B-concrete under quasi-static loading while the specimen 1C1B and 1B1C showed similar results of debonding loads under dynamic loadings. Under quasi-static loading, the higher bond strength was resulted from the relatively higher stiffness of CFRP sheets which were directly bonded to concrete substrates. There was a consistent finding that the bond strength correlates well with FRP stiffness as well as concrete tensile strength, consequently the bond strength is mainly determined by the FRP layer which is directly attached to the concrete substrate [24]. The influence of FRP stacking sequence on the bond strength should be resulted from the shear stress redistribution within the FRP interlayers. Under quasi-static loading, the average debonding load of Specimen QBC was 11.04 kN while its counterpart (i.e., QCB) was 10.55 kN. However, the impact of FRP stacking sequence on the bond strength is marginal when the loading speed is over 1 m/s, which indicates that effect of strain rate on the bond strength is more prominent than the FRP stacking sequence under dynamic loadings. This is due to the enhanced tensile strengths of concrete and epoxy under dynamic loading which results in the increment of interfacial bond strength.

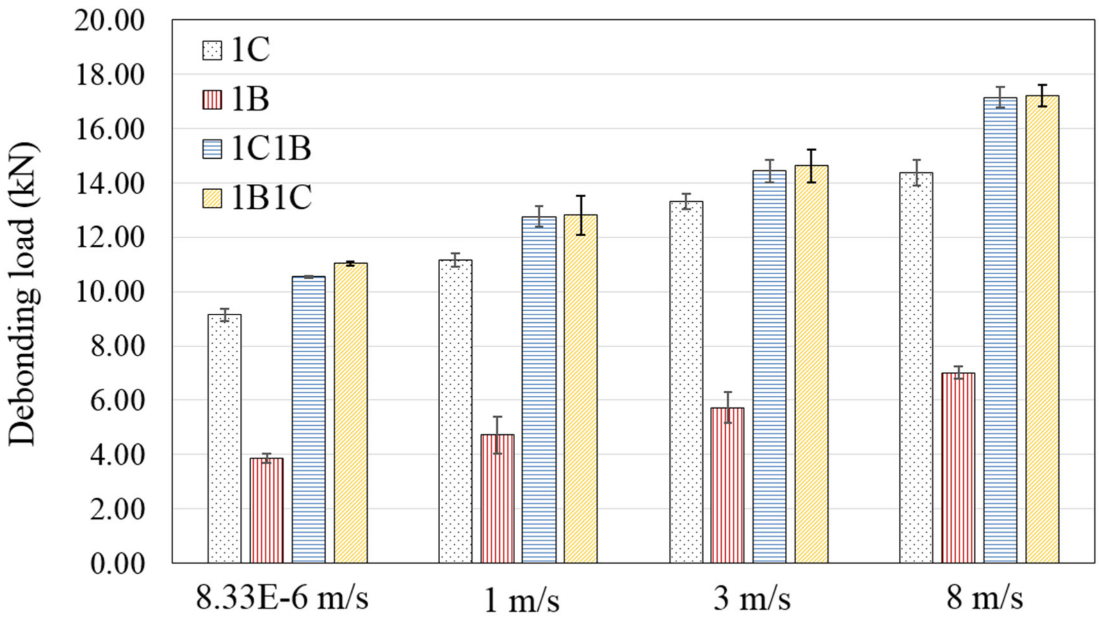

Figure 6. Comparison of debonding load

3.2 Strain time history and stress equilibrium

The strain contours of the tested specimens at the loading rate of 1 m/s are plotted in Figure 7, which consist of different colours (i.e., red, yellow, green, light blue, and dark blue) showing the strain distributions at different loading levels. With the increase of the applied load, the strain gradient in red colour continued to develop and propagate along the FRP sheets. The region with the colours of yellow, green and light blue represents the shear stress transfer zone and the dark blue represents the non-stress transfer zone. At the initial debonding stage (i.e., *P*), a large local strain gradient shown in red colour was observed close to the loaded end. As compared with the sole FRP (i.e., 1C and 1B), the hybrid composites (i.e., 1C1B and 1B1C) show a larger range of shear stress transfer zone at the initial debonding stage (i.e., *P*), indicating that the relative slippage occurred between CFRP and BFRP sheets due to their different stiffness.

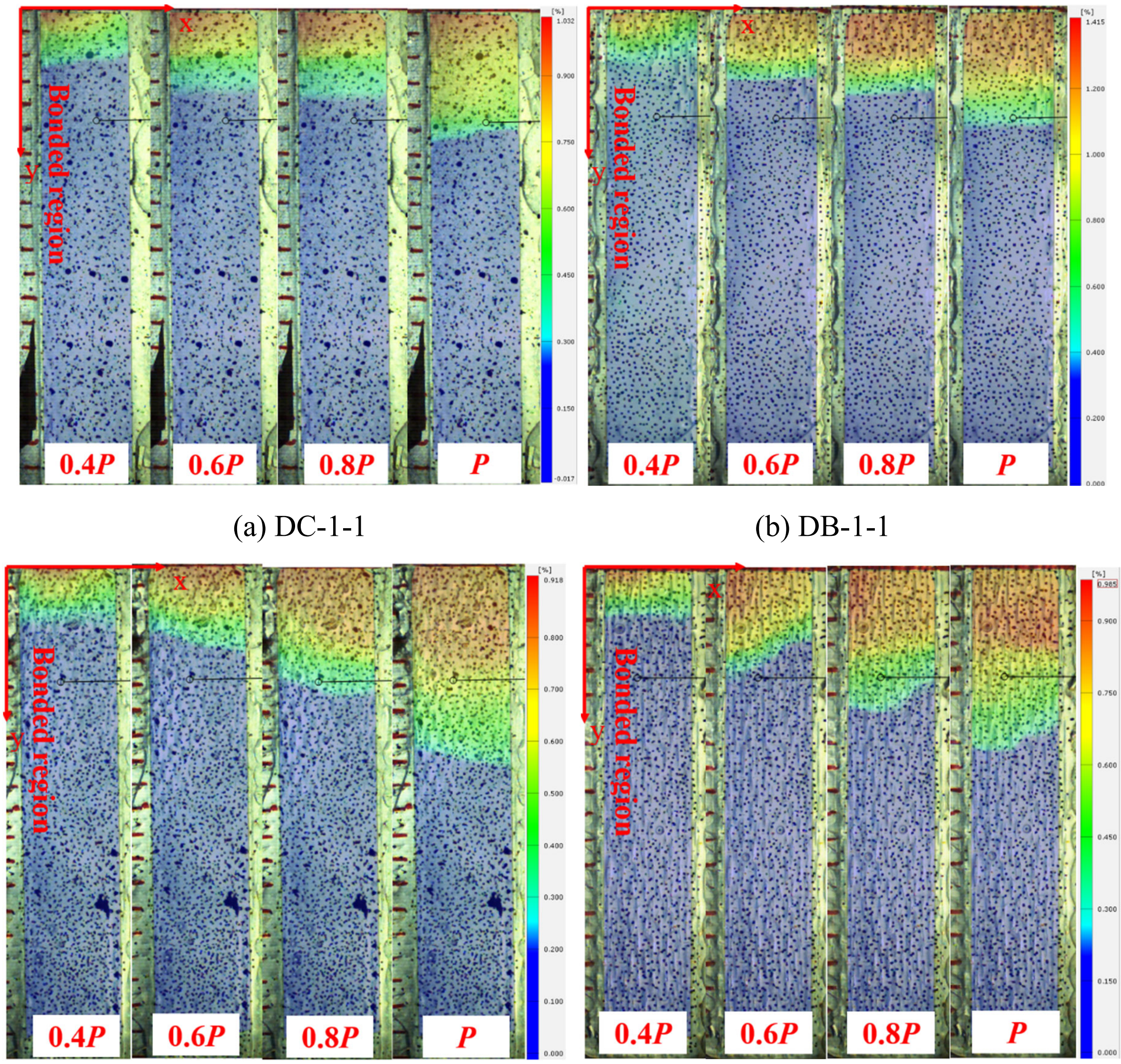

(a) DC-1-1 (b) DB-1-1

(c) DCB-1-1 (d) DBC-1-1

Figure 7. Strain contours of the tested specimens

Figure 8 plots the strain time-history curves at different loading speeds. The average values of all the testing results are shown in Figure 9. The general trend of the testing results shows that the ultimate debonding strain increased with the rising strain rate. Due to the high loading rate and short-time loading, the strain time-history curves under high loading speed become steeper as compared to those under low loading velocity. Compared with the 1C-concrete interface, the interface of 1B-concrete is more sensitive to strain rate due to the significant increment of the ultimate debonding strain. The ultimate debonding strain of the 1B-concrete interface increased by 84% from 0.98% at the strain rate of 2.5E-5 s^{-1} to 1.80% at the strain rate of 155

s^{-1} while the ultimate debonding strain of the 1C-concrete interface increased by 35% from 0.78% to 1.05% when the strain rate increased from 2.5E-5 s^{-1} to 128 s^{-1}, respectively. It can be concluded that 1C-concrete interface is less sensitive to strain rate as the stiffer CFRP is lack of strain rate sensitivity as also observed in the previous study [25].

For the hybrid composites (i.e., 1C1B and 1B1C), the ultimate debonding strain decreased significantly as compared to 1B-concrete interface under all the corresponding loading velocities, indicating that an addition of a CFRP sheet resulted in the decreased debonding strain. This observation under high loading rate agrees well with the well-known behaviour under quasi-static loads, where the thicker FRP sheets show a lower debonding strain [13]. The reduction of the ultimate debonding strain indicates that the enhancement of shear resistance between FRP and concrete caused by the increased FRP stiffness ($E_f t_f$). Additionally, the stacking sequence of FRP sheets resulted in different ultimate strain at the quasi-static loading while the effect of stacking sequence on the ultimate debonding strain was marginal under dynamic loadings. The 1C1B-concrete interface resulted in a relatively higher ultimate strain than its counterpart (1B1C-concrete interface) at the quasi-static loading, as shown in Figure 9. However, the FRP stacking sequence had a marginal effect on the ultimate debonding strain under dynamic loading, which is shown in Figure 9. The possible reason is that there is not enough time for the shear stress to be redistributed in the FRP interlayers under dynamic loading.

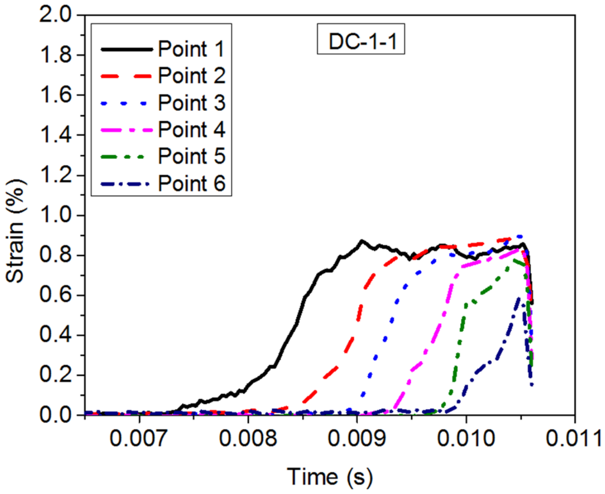
DC-1-1
Point 1
Point 2
Point 3
Point 4
Point 5
Point 6
Strain (%)
Time (s)

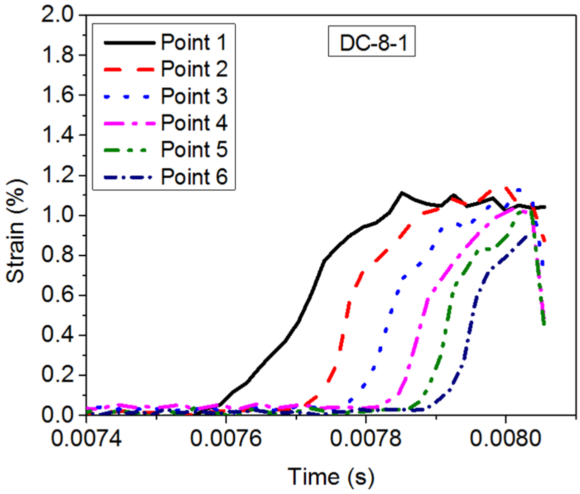
DC-8-1
Point 1
Point 2
Point 3
Point 4
Point 5
Point 6
Strain (%)
Time (s)

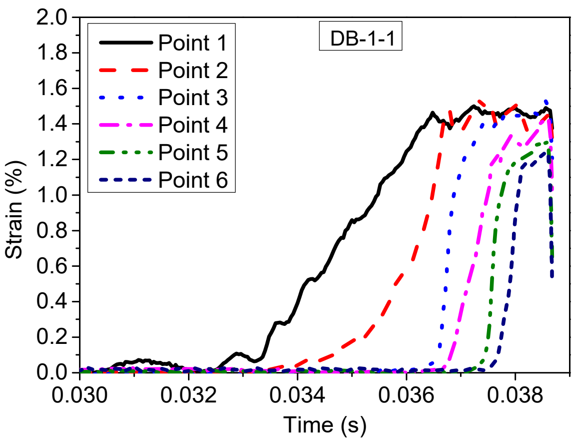
DB-1-1
Point 1
Point 2
Point 3
Point 4
Point 5
Point 6
Strain (%)
Time (s)

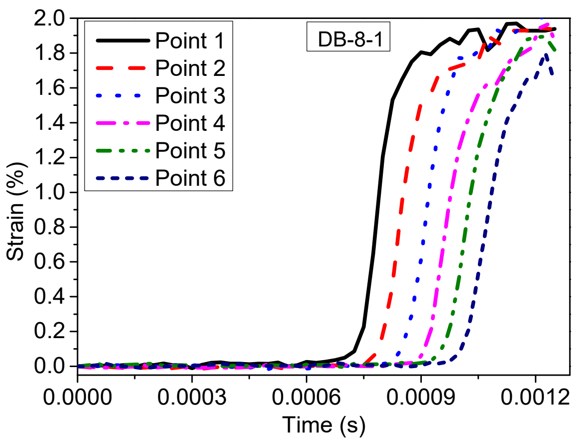
DB-8-1
Point 1
Point 2
Point 3
Point 4
Point 5
Point 6
Strain (%)
Time (s)

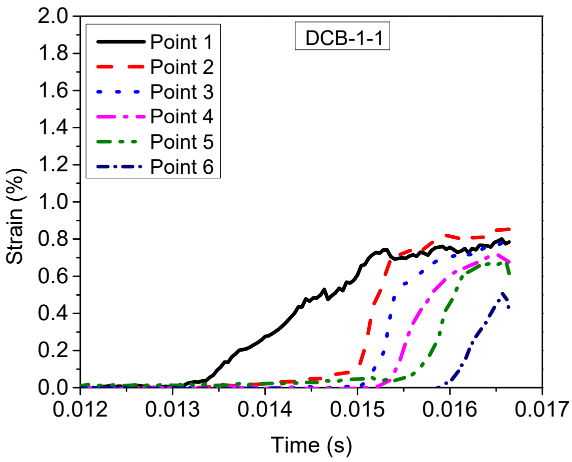
DCB-1-1
Point 1
Point 2
Point 3
Point 4
Point 5
Point 6
Strain (%)
Time (s)

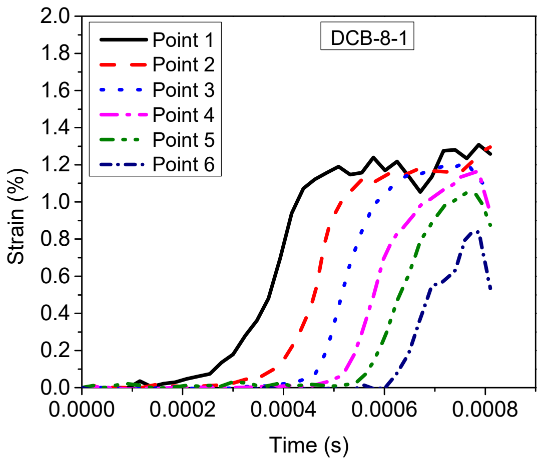
DCB-8-1
Point 1
Point 2
Point 3
Point 4
Point 5
Point 6
Strain (%)
Time (s)

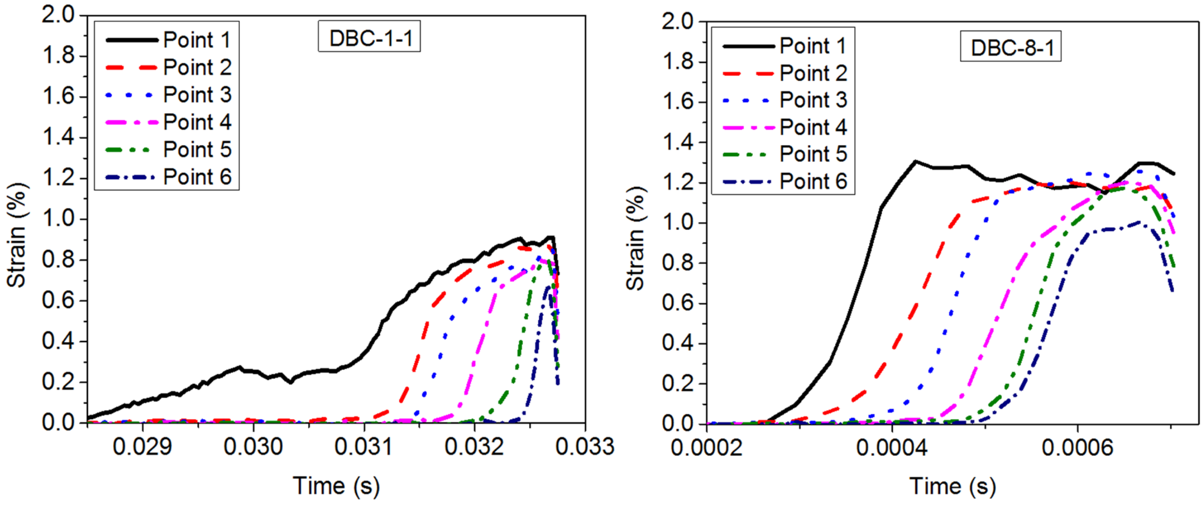

Figure 8. Strain time history at different loading rates

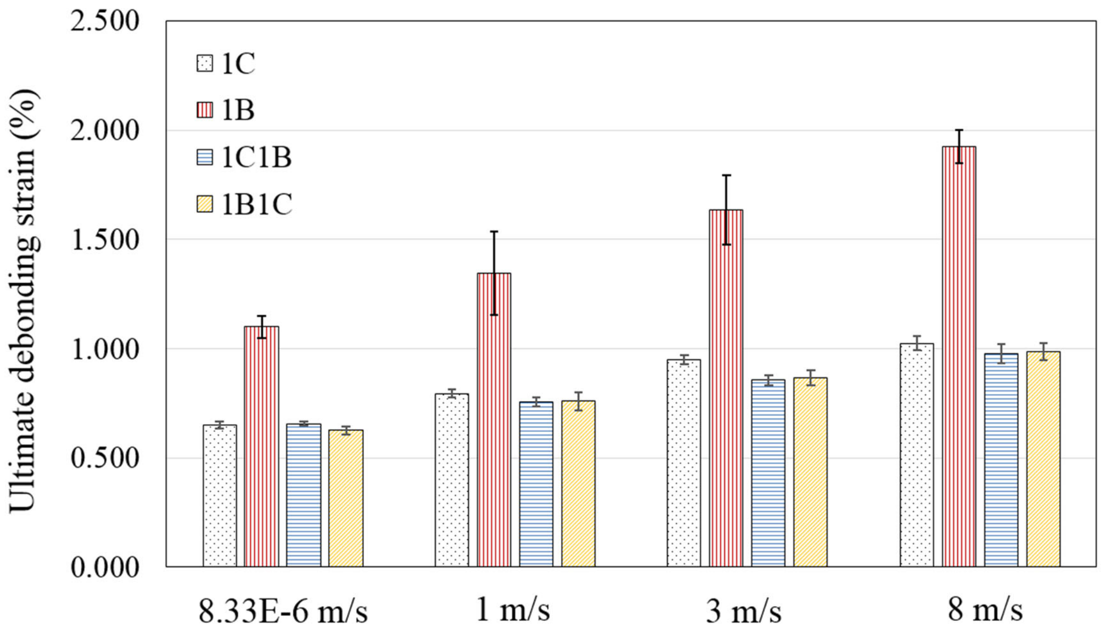

Figure 9. Comparison of ultimate debonding strain

To obtain valid testing results, the dynamic stress equilibrium must be achieved in the dynamic test [1, 26]. The elastic stress wave velocity can be obtained by using equation $c=\sqrt{\frac{E}{\rho}}$, but the elastic modulus and density cannot be identified for the interface due to three components (i.e., FRP, concrete and epoxy resin) are involved. Therefore, six points along the centreline of the FRP as shown in Figure 1 (a) are selected to compare the strain time-history curves. Figure 8 plots the strain time-history curves of the tested specimens under different loading velocities.

The strain curves developed a similar and uniform plateau for all the cases, indicating that the stress equilibrium was achieved.

Figure 10 plots the strain rate distributions along the FRP sheet at different time instants. The strain rate in this study was derived by differentiating the strain time history using the equation $\dot{\varepsilon} = \frac{d\varepsilon}{dt}$. As labelled in Figure 10, the peak strain rate was defined as the measured strain rate for each test in this study. All the tested specimens exhibited a similar pattern of propagation from the loaded end to the free end. The peak strain rate increases with the rising loading rate and the peak strain rate for DCB-1-1 and DCB-8-1 is 16.89 s^{-1} and 98.21 s^{-1}, respectively. The peak strain rate of each specimen is summarized in Table 2.

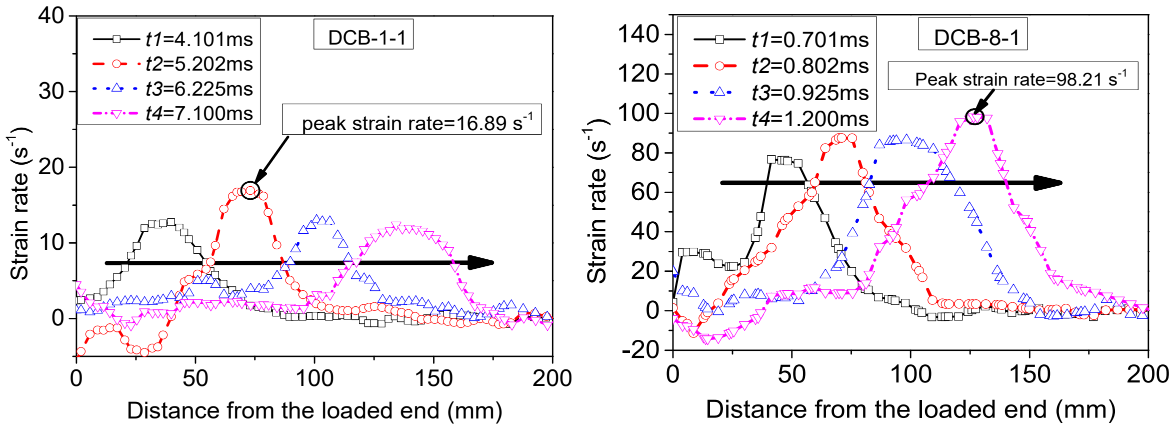

Figure 10. Strain rate of the tested specimens

3.3 Strain distributions

Figure 11 shows the strain profile along the centreline of FRP at different loading stages. It is found that the strain rate effect on the strain distributions is more prominent than the hybrid effect because the FRP debonding strain increased noticeably with strain rate. For hybrid composite-concrete interface, an additional layer of FRP sheet resulted in a lower ultimate debonding strain compared with the sole FRP-concrete interface at each loading rate. This is consistent with previous studies that the thicker FRP sheets cause the reduction of debonding strain [18]. Additionally, the stacking sequence of FRP sheets gave rise to different ultimate debonding strains for hybrid FRP composites. The attachment of CFRP sheets (i.e., 1B1C) first to the concrete substrate caused a relatively higher initial debonding strain under quasi-static loading as compared to the attachment of BFRP sheet (i.e., 1C1B) first. However, the effect of stacking sequence on the ultimate strain was marginal with the increasing strain rate because similar ultimate debonding strain of hybrid composites was observed under dynamic loadings. The shear stress developed in the composite is proportional to the debonding strain and consequently the higher debonding strain resulted in higher interfacial shear stress.

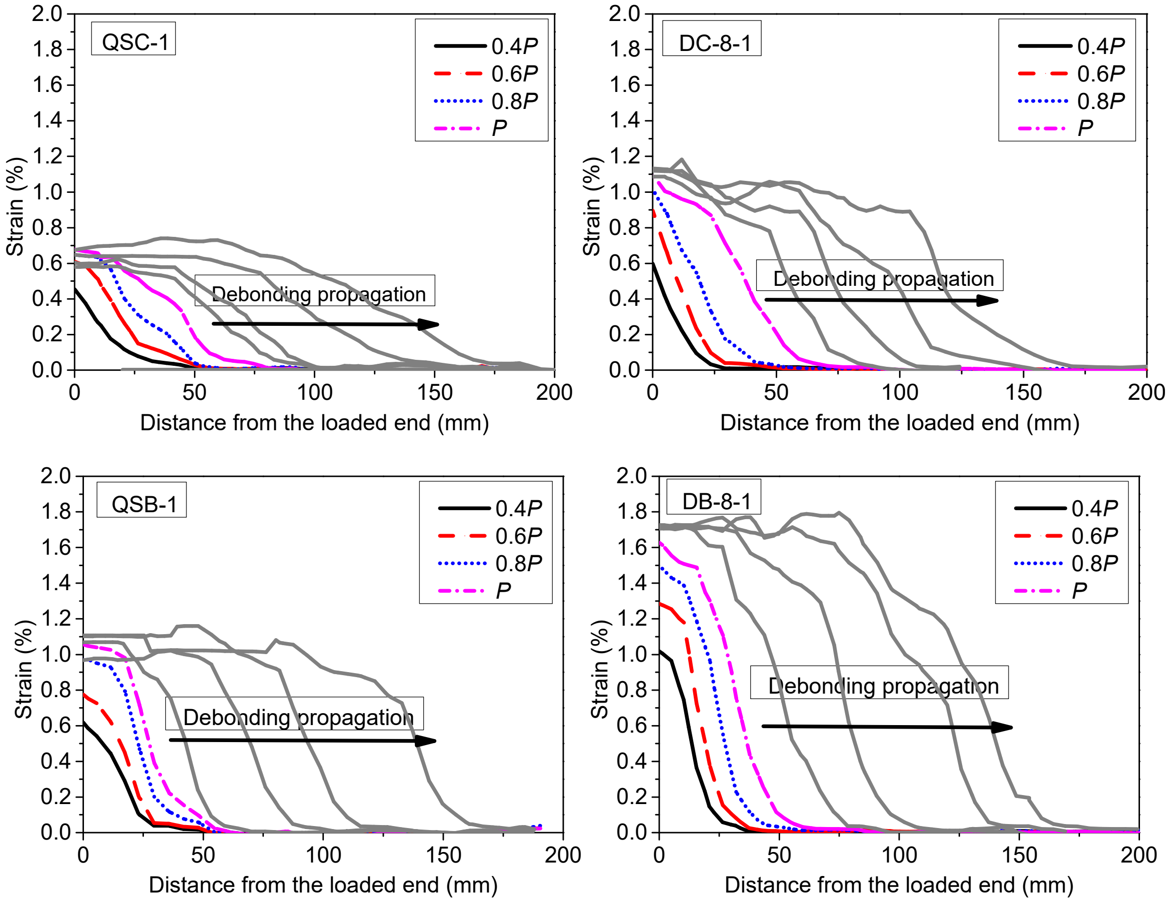

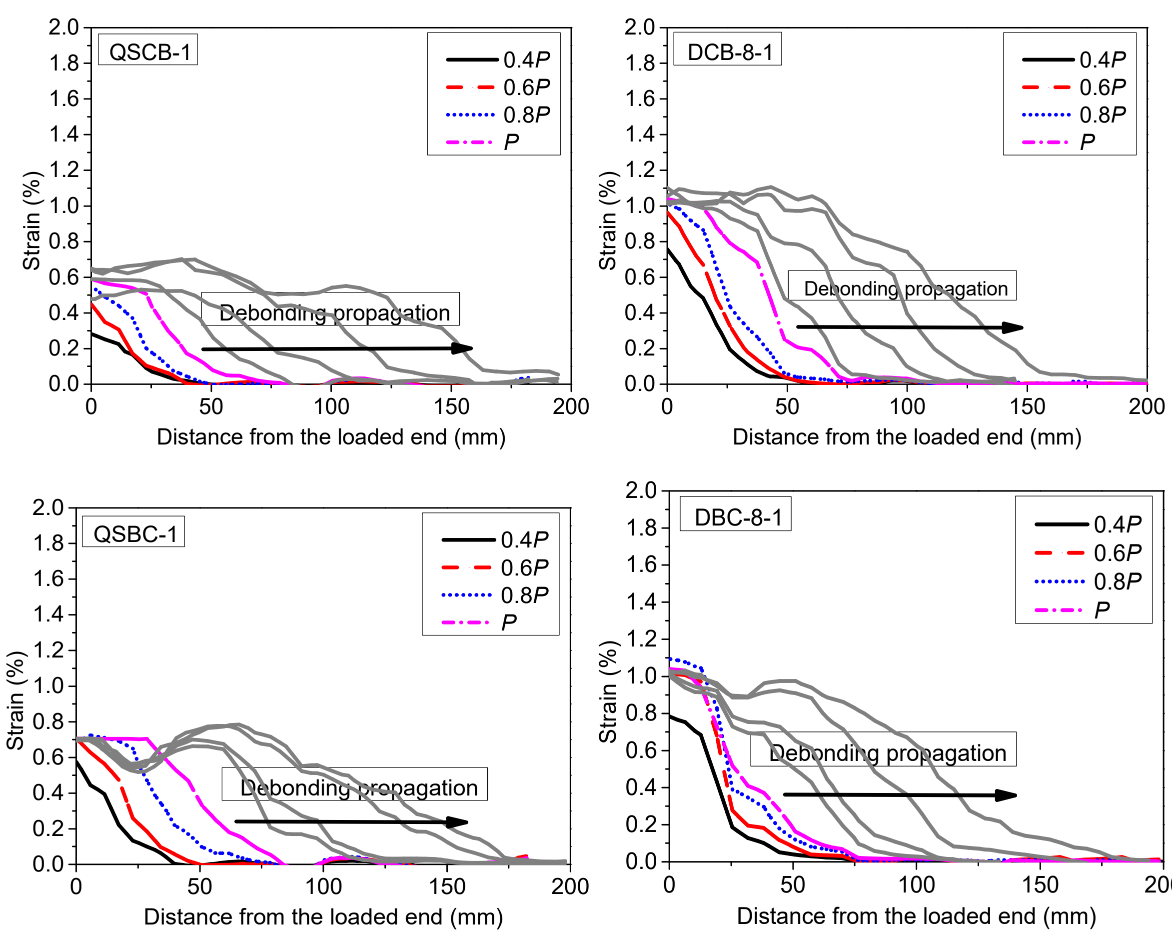

Figure 11. Typical strain distributions

The ultimate debonding strain at the initial debonding load *P* raised with strain rate while the range of stress transition zone reduced with the increasing strain rate. This is because the strain distribution gradient in the FRP was steeper than that under quasi-static loading, as shown in Figure 12. Equation (1) was used to fit the experimental strain profiles under different loading speeds and loading levels [27]. The steeper strain distribution gradient means a shorter stress transition zone, which is also known as the effective bond length (EBL) [24, 28]. It was observed that the EBL reduced with the rising strain rate. The decrease of the effective bond length was resulted from the increase of the interfacial shear stress with the increase of loading rate. The dynamic tensile strength of concrete increased with strain rate due to the dynamic increase factor (DIF) [29]. As a result, the EBL decreased with the increasing loading rate, which is consistent with the previous study [18]. The hybrid composites DCB-8-1 and DBC-

8-1 showed an approximately similar EBL at the loading rate of 8 m/s as shown in Figure 12 (b), indicating that the stacking sequence has a marginal impact on the effective bond length under relatively higher loading rate. This is because there is not enough time for FRP sheets to develop the relative slippage in the interlayers of hybrid composites at relatively higher strain rate. The strain of FRP sheets can be estimated by the following equation:

$$\varepsilon(x) = \varepsilon_u + \frac{A}{1+e^{\left(\frac{x-x_o}{B}\right)}} \tag{1}$$

in which A and B are regression coefficients, x is the distance of the bonded BFRP sheet from 0 to 200 mm, x_o is the turning point of strain distribution as shown in Figure 12, and ε_u is the experimental ultimate debonding strain as listed in Table 2. The best fit coefficients A and B are summarized in Table 2.

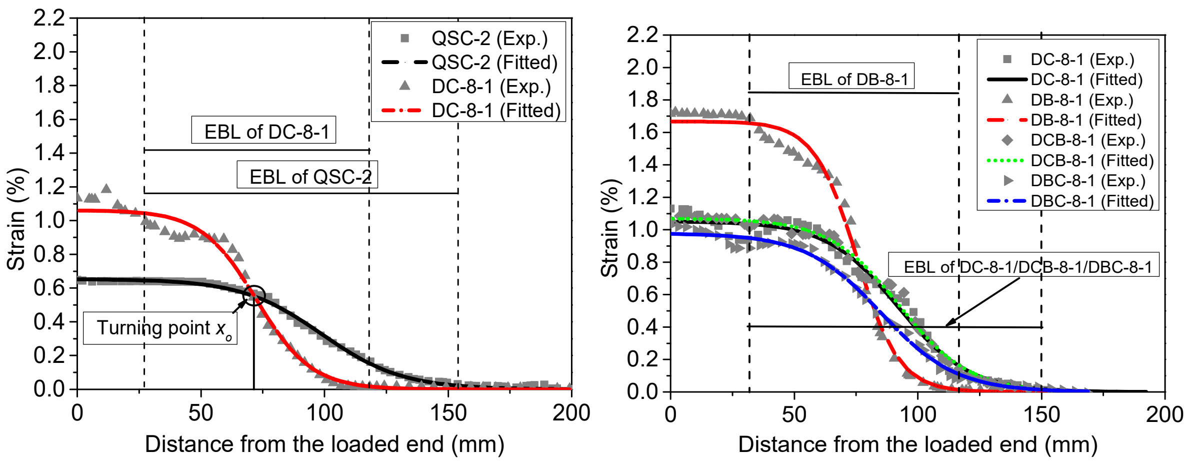

Figure 12. Effective bond length of the tested specimens

3.4 Bond-slip response

The relationship between the interfacial shear stress and the corresponding shear slip along the FRP sheets are discussed in this section. By assuming the zero relative slip between concrete and FRP at the free end before the final debonding as shown in Figure 1, the shear slip can be obtained by the integration of the measured strain profile along the FRP sheets:

$$s(x)=\int \varepsilon dx \tag{2}$$

The axial FRP strain was measured by the DIC technique, thus, the interfacial shear stress can be obtained using the following equation [23]:

$$\tau(x)=E_f t_f \frac{d\varepsilon}{dx} \tag{3}$$

in which $s(x)$ is the shear slip, $\tau(x)$ is the shear stress, ε is the BFRP strain, and $E_f t_f$ is the BFRP stiffness. Typical interfacial bond-slip curves of the tested specimens are shown in Figure 13. In order to obtain the mean shear stress and the slip, five different points after the initial debonding stage (i.e., *P*) are selected as shown in the legend, such as 65 mm and 185 mm. Both the ascending branch and the descending branch can be observed for all the specimens. The non-linear bond-slip response was resulted from the cracking of concrete. The general trend of the bond-slip response shows that the interfacial peak shear stress τ_m raised remarkably with strain rate. By comparing the testing results of the 1C-concrete and the 1B-concrete interface, it is found that the peak shear stress was significantly influenced by the FRP stiffness ($E_f t_f$). It is noted that the strength of concrete is also an important factor to determine the interfacial shear stress, which has been discussed in the previous studies [23].

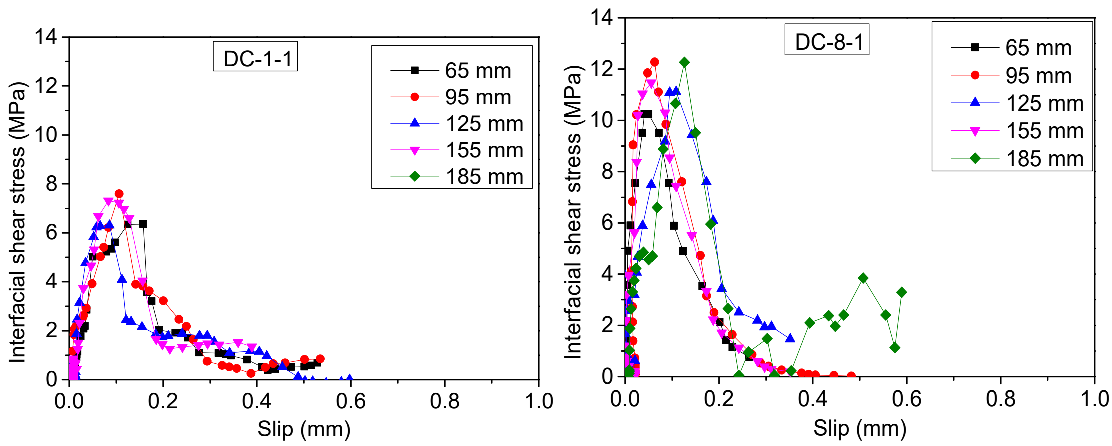

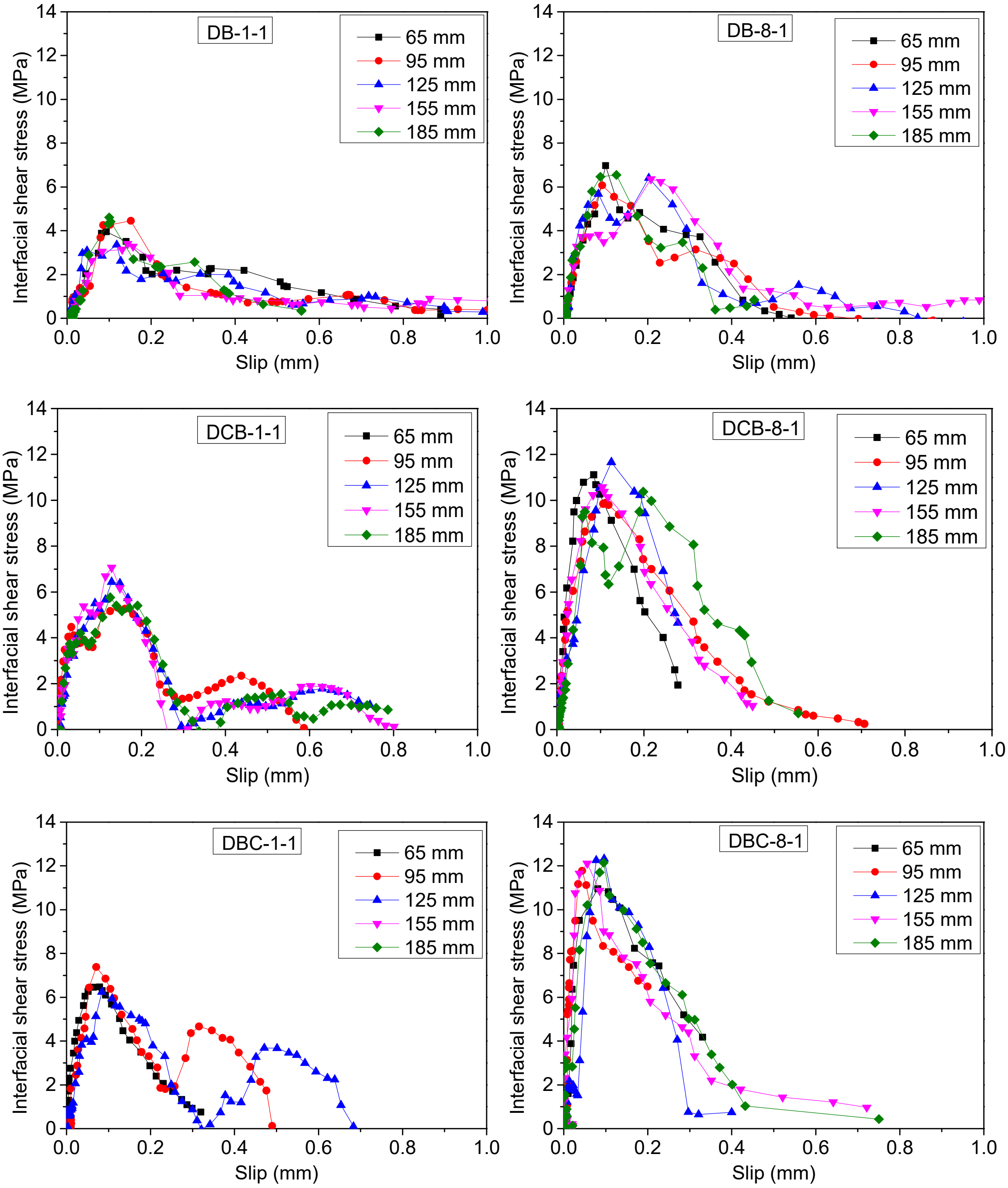

Figure 13. Typical bond-slip curves

Figure 14 illustrates the comparison of the peak shear stress. It is found that the 1C-concrete interface showed higher interfacial shear stress than the 1B-concrete interface. The hybrid composites with the same FRP stiffness showed higher shear stress than sole FRP under the quasi-static loading. This trend was also observed for the hybrid composites at which the peak shear stress of the 1B1C-concrete interface showed higher shear stress than its counterpart (i.e., 1C1B-concrete) under dynamic loadings from 1 m/s to 8 m/s. The increased interfacial shear stress was caused by the enhanced interfacial stiffness, which correlates well with the shear modulus of concrete and FRP sheets. An increment of 191%, 226%, 144%, and 157% in shear stress from quasi-static loading to 8 m/s dynamic loading was obtained for Specimen DC-8, DB-8, DCB-8, and DBC-8, respectively. The combination of CFRP and BFRP sheet not only made the hybrid composites sensitive to strain rate, but also enhanced the shear resistance. The enhanced shear stress for hybrid composites should be resulted from the increased FRP stiffness and the enhanced concrete strength. At the largest loading speed, the peak shear stress between the 1C-concrete, 1C1B-concrete, and 1B1C-concrete interfaces were similar, indicating that the interfacial shear stress was more sensitive to strain rate than the hybrid effect under dynamic loadings. At the same loading rate, the 1B-concrete interface had a relatively low peak shear stress due to its low stiffness (i.e., 1B had the stiffness of 8.76 N/mm).

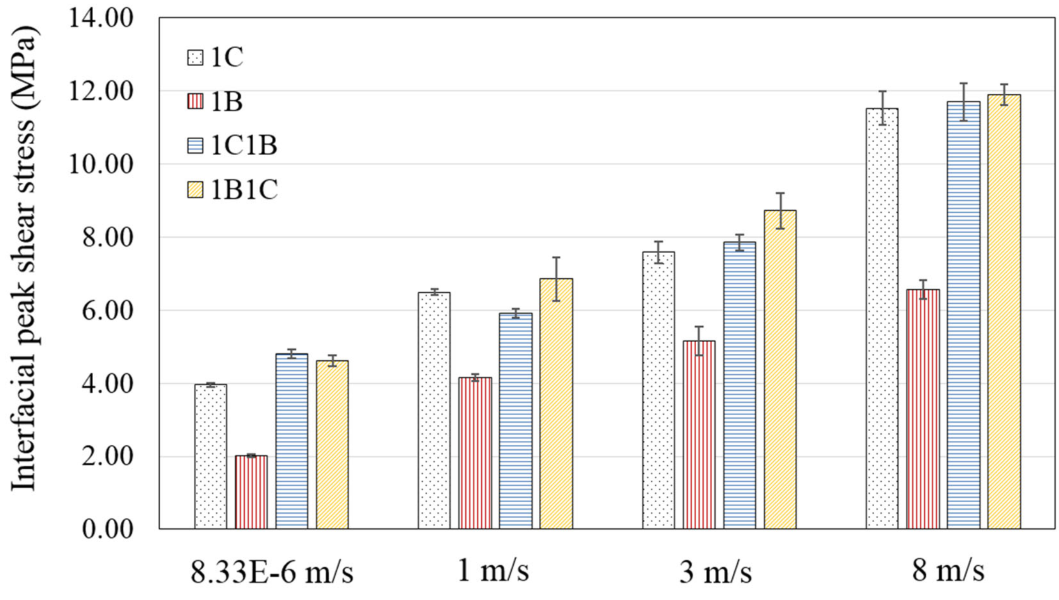

Figure 14. Interfacial peak shear stress at different loading rates

Figure 15 compares the interfacial fracture energy (G_f) of the FRP-to-concrete interface, which can be obtained from the enclosed area of the bond-slip curve [30]. Due to the fluctuated bond-slip curves, the obtained G_f showed high dispersion, as indicated in the error bar of the experimental results in Figure 15. In general, the test results show that the G_f raised significantly with strain rate for all the specimens. This is due to the increased tensile strength of concrete and previous studies have demonstrated that the G_f was proportional to the tensile strength of concrete and FRP stiffness [30]. The specimen 1C1B-concrete interface had a relatively higher fracture energy than that of specimen 1B1C-concrete interface under the quasi-static loading, indicating that the attachment of BFRP sheet first to concrete substrate caused a relatively higher fracture energy. However, the hybrid effect on the fracture energy was marginal for hybrid composites under the dynamic loadings from 1 m/s to 8 m/s as both the 1C1B-concrete and 1B1C-concrete interfaces showed a similar result. As the hybrid effect should be resulted from the stress redistributions within the internal layers between FRP sheets, there is not enough time for the shear stress to redistribute due to the increased strain rate. The G_f of hybrid composites is slightly higher than the sole FRP sheet in general.

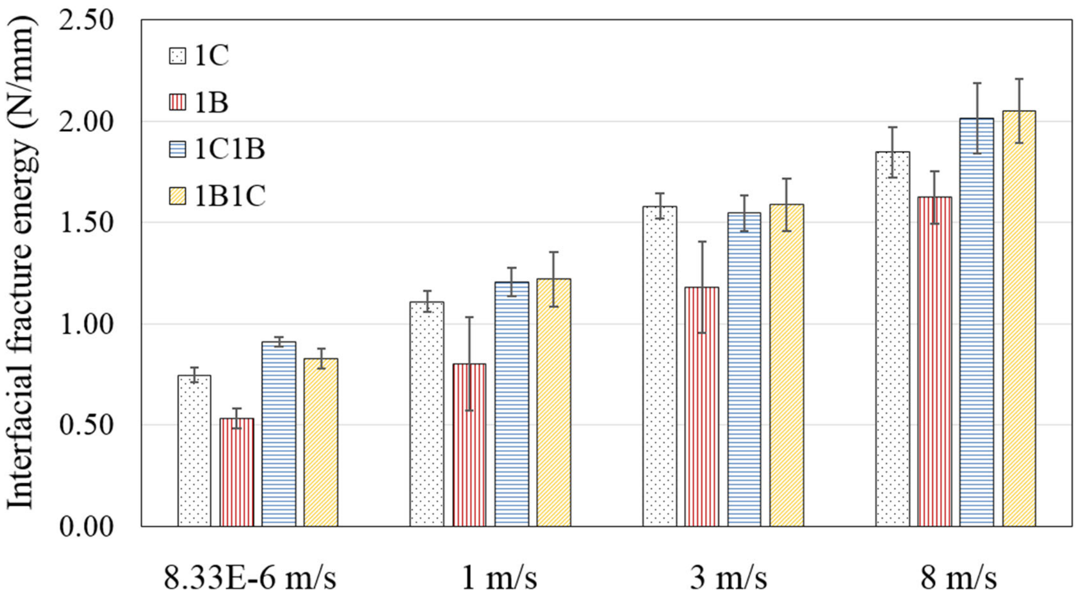

Figure 15. Comparison of G_f

3.5 Dynamic bond strength and shear stress

3.5.1 Strain rate effect on interfacial bond strength

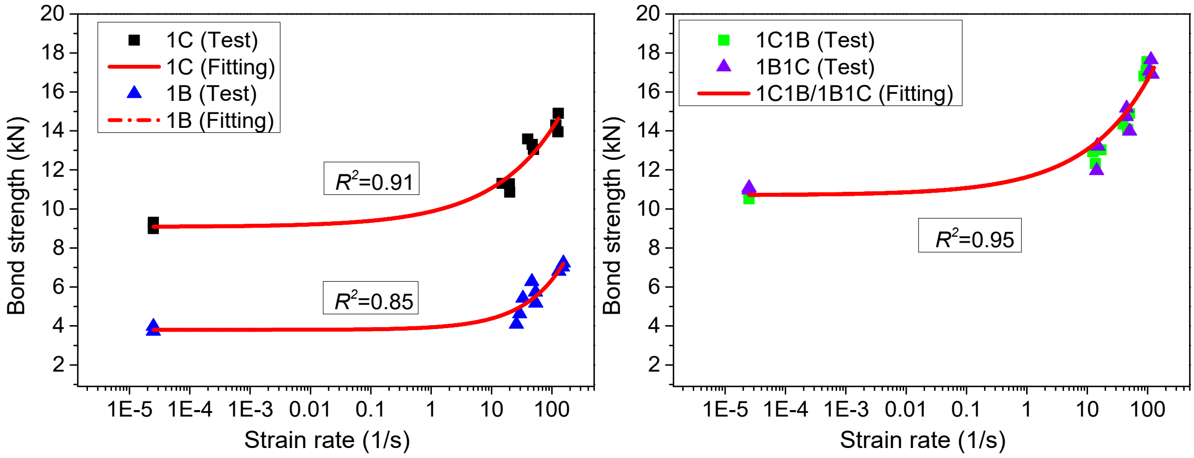

Figure 16. Interfacial bond strength vs. strain rate

Figure 16 plots the interfacial bond strength versus strain rate. The average quasi-static bond strength is 9.15 kN, 3.86 kN, 10.55 kN and 11.04 kN for 1C, 1B, 1C1B and 1B1C, respectively. The bond strength of all the specimens increases with the strain rate. The bond strength of specimen 1C at the strain rate of 127.97 s^{-1} is 14.90 kN, increased by 62.8% as compared to the quasi-static one. The bond strength of specimen 1C1B is 17.55 kN at the strain rate of 98.21 s^{-1}, increased by 66.4% as compared to the quasi-static one. For ease of comparison, the testing data and fitted curves of specimens 1C and 1B are grouped in Figure 16 (L) and Figure 16 (R) shows the testing data and fitted curves of the specimens 1C1B and 1B1C. To predict the dynamic interfacial bond strength of FRP-concrete interface, empirical formulae are proposed and expressed as follows. It should be noted that single empirical formula is proposed for the specimens 1C1B and 1B1C since they have very similar strain rate effect on the bond strength.

For 1C,

$$P_{d,C} = P_{s,C}\left[0.086(\dot{\varepsilon})^{0.402} + 0.992\right] \quad \text{when } 2.5\times10^{-5} \le \dot{\varepsilon} \le 128 \qquad (4)$$

For 1B,

$$P_{d,B} = P_{s,B}\left[0.034(\dot{\varepsilon})^{0.645} + 0.986\right] \text{ when } 2.5\times10^{-5} \le \dot{\varepsilon} \le 155 \quad (5)$$

For 1C1B and 1B1C,

$$P_{d,CB} = P_{s,CB}\left[0.039(\dot{\varepsilon})^{0.577} + 0.998\right] \text{ when } 2.5\times10^{-5} \le \dot{\varepsilon} \le 119 \quad (6)$$

3.5.2 Strain rate effect on interfacial shear stress

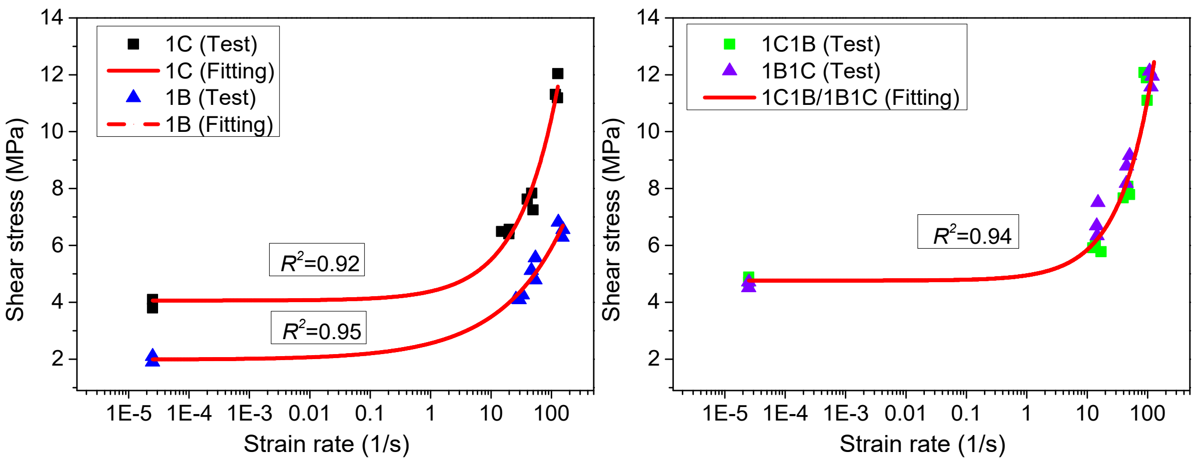

Figure 17. Interfacial shear stress vs. strain rate

Figure 17 illustrates the relationship of the interfacial shear stress versus strain rate. The average quasi-static shear stress is 3.95 MPa, 2.01 MPa, 4.80 MPa and 4.62 MPa for 1C, 1B, 1C1B and 1B1C, respectively. The shear stress of specimen 1C, 1B, 1C1B and 1B1C at the strain rate of 127.97 s^{-1}, 155.10 s^{-1}, 98.21 s^{-1} and 118.96 s^{-1} is 14.90 MPa, 7.23 MPa, 17.55 MPa and 16.91 MPa, with the increment of 277%, 226%, 144% and 157% as compared to the quasi-static one, respectively. Figure 17 (L) illustrates the testing data and fitted curves of the specimens 1C and 1B and Figure 17 (R) shows the experimental results and fitting curves of the specimens 1C1B and 1B1C. As the hybrid composites 1C1B and 1B1C exhibit similar strain rate effect on shear stress, single empirical formula is proposed for them. The empirical formulae to predict dynamic shear stress are given as follows.

For 1C,

$$\tau_{d,C} = \tau_{s,C}\left[0.081(\dot{\varepsilon})^{0.649} + 1.028\right] \text{ when } 2.5\times10^{-5} \le \dot{\varepsilon} \le 128 \quad (7)$$

For 1B,

$$\tau_{d,B} = \tau_{s,B}\left[0.286(\dot{\varepsilon})^{0.417} + 0.987\right] \text{ when } 2.5\times10^{-5} \le \dot{\varepsilon} \le 155 \quad (8)$$

For 1C1B and 1B1C,

$$\tau_{d,CB} = \tau_{s,CB}\left[0.041(\dot{\varepsilon})^{0.772} + 1.014\right] \text{ when } 2.5\times10^{-5} \le \dot{\varepsilon} \le 119 \quad (9)$$

4. Conclusions

In this study, the single-lap shear tests were conducted to investigate the dynamic interfacial bond behaviour between hybrid carbon/basalt FRP sheet and concrete under the loading rates of 8.33E-6 m/s, 1 m/s, 3 m/s, and 8 m/s, corresponding to the strain rate between 2.50E-5 s^{-1} and 155.10 s^{-1}, the following conclusions can be drawn:

(1) The debonding failure surface changed from concrete substrate to the interface between adhesive and concrete and a combined failure mode was observed with the rising strain rate for both sole and hybrid composites.

(2) The debonding load increased remarkably with the strain rate for both the sole and hybrid composites. An additional layer of FRP sheet for hybrid composites enhanced the bond strength. The stacking sequence of FRP sheets resulted in different bond strength under quasi-static loading while the effect of stacking sequence on bond strength was marginal when the loading rate is over 1 m/s. Empirical formulae were proposed to predict the dynamic interfacial bonding strength and shear stress.

(3) The 1B-concrete interface showed higher strain rate sensitivity than that of the 1C-concrete interface due to the significant increment of ultimate debonding strain. An additional layer

of FRP sheet for hybrid composites led to the reduction of ultimate debonding strain due to the increased stiffness.

(4) The stress transfer zone reduced with the increasing strain rate. The stacking sequence of FRP sheet affected the stress transfer zone due to the shear stress redistribution in the interlayers under static loads, while the stress transfer zone of hybrid composites showed similar results at the highest considered loading speed of 8 m/s.

(5) Strain rate effect on the bond-slip response was more significant than the hybrid effect with the increasing loading rate because of the enhanced tensile strength of concrete. The interface between hybrid composites and concrete showed higher peak shear stress and interfacial fracture energy than that of sole FRP at same loading rate.

Acknowledge

The authors thank the Australian Research Council Linkage Project (LP150100259) for financial support.

References

[1] Chen W, Hao H, Jong M, Cui J, Shi Y, Chen L, et al. Quasi-static and dynamic tensile properties of basalt fibre reinforced polymer. Compos B Eng. 2017;125:123-33.
[2] Meshgin P, Choi K-K, Taha MMR. Experimental and analytical investigations of creep of epoxy adhesive at the concrete–FRP interfaces. Int J Adhes Adhes. 2009;29(1):56-66.
[3] Mukhtar FM, Faysal RM. A review of test methods for studying the FRP-concrete interfacial bond behavior. Constr Build Mater. 2018;169:877-87.
[4] Ferracuti B, Savoia M, Mazzotti C. Interface law for FRP–concrete delamination. Compos Struct. 2007;80(4):523-31.
[5] Zhang H, Smith ST. Influence of plate length and anchor position on FRP-to-concrete joints anchored with FRP anchors. Compos Struct. 2017;159:615-24.
[6] Swolfs Y, Gorbatikh L, Verpoest I. Fibre hybridisation in polymer composites: a review. Composites Part A: Applied Science and Manufacturing. 2014;67:181-200.
[7] Marom G, Fischer S, Tuler F, Wagner H. Hybrid effects in composites: conditions for positive or negative effects versus rule-of-mixtures behaviour. J Mater Sci. 1978;13(7):1419-26.
[8] Naik N, Ramasimha R, Arya H, Prabhu S, ShamaRao N. Impact response and damage tolerance characteristics of glass–carbon/epoxy hybrid composite plates. Compos B Eng. 2001;32(7):565-74.

[9] Ribeiro F, Sena-Cruz J, Branco FG, Júlio E. Hybrid effect and pseudo-ductile behaviour of unidirectional interlayer hybrid FRP composites for civil engineering applications. Constr Build Mater. 2018;171:871-90.
[10] Kim HS, Shin YS. Flexural behavior of reinforced concrete (RC) beams retrofitted with hybrid fiber reinforced polymers (FRPs) under sustaining loads. Compos Struct. 2011;93(2):802-11.
[11] Li L, Guo Y, Liu F. Test analysis for FRC beams strengthened with externally bonded FRP sheets. Constr Build Mater. 2008;22(3):315-23.
[12] Choi E, Utui N, Kim HS. Experimental and analytical investigations on debonding of hybrid FRPs for flexural strengthening of RC beams. Compos B Eng. 2013;45(1):248-56.
[13] Yuan C, Chen W, Pham TM, Hao H. Bond behaviour between hybrid fiber reinforced polymer sheets and concrete. Constr Build Mater. 2019;210:93-110.
[14] Pham TM, Hao H. Behavior of fiber-reinforced polymer-strengthened reinforced concrete beams under static and impact loads. International Journal of Protective Structures. 2017;8(1):3-24.
[15] Buchan P, Chen J. Blast resistance of FRP composites and polymer strengthened concrete and masonry structures–A state-of-the-art review. Compos B Eng. 2007;38(5-6):509-22.
[16] Giannis S, Adams RD. Failure of elastomeric sealants under tension and shear: Experiments and analysis. Int J Adhes Adhes. 2019.
[17] Yuan C, Chen W, Pham TM, Hao H, Cui J, Shi YC. Strain rate effect on interfacial bond behaviour between BFRP sheets and steel fibre reinforced concrete. Compos B Eng. 2019.
[18] Huo J, Liu J, Lu Y, Yang J, Xiao Y. Experimental study on dynamic behavior of GFRP-to-concrete interface. Eng Struct. 2016;118:371-82.
[19] Salimian MS, Mostofinejad D. Experimental Evaluation of CFRP-Concrete Bond Behavior under High Loading Rates Using Particle Image Velocimetry Method. J Compos Constr. 2019;23(3):04019010.
[20] Karachalios E, Adams R, da Silva LF. Strength of single lap joints with artificial defects. Int J Adhes Adhes. 2013;45:69-76.
[21] Yuan C, Chen W, Pham TM, Hao H. Bond behavior between basalt fibres reinforced polymer sheets and steel fibres reinforced concrete. Eng Struct. 2018;176:812-24.
[22] Teng J, Yuan H, Chen J. FRP-to-concrete interfaces between two adjacent cracks: Theoretical model for debonding failure. Int J Solids Struct. 2006;43(18-19):5750-78.
[23] Wu Y-F, Jiang C. Quantification of bond-slip relationship for externally bonded FRP-to-concrete joints. J Compos Constr. 2013;17(5):673-86.
[24] Hosseini A, Mostofinejad D. Effective bond length of FRP-to-concrete adhesively-bonded joints: Experimental evaluation of existing models. Int J Adhes Adhes. 2014;48:150-8.
[25] Bunsell A, Harris B. Hybrid carbon and glass fibre composites. Composites. 1974;5(4):157-64.
[26] Chen W, Hao H, Hughes D, Shi Y, Cui J, Li Z-X. Static and dynamic mechanical properties of expanded polystyrene. Materials & Design. 2015;69:170-80.
[27] Ali-Ahmad M, Subramaniam K, Ghosn M. Experimental investigation and fracture analysis of debonding between concrete and FRP sheets. J Eng Mech. 2006;132(9):914-23.
[28] Ouezdou MB, Belarbi A, Bae S-W. Effective bond length of FRP sheets externally bonded to concrete. Int J Concr Struct M. 2009;3(2):127-31.
[29] Cui J, Hao H, Shi Y. Discussion on the suitability of concrete constitutive models for high-rate response predictions of RC structures. International Journal of Impact Engineering. 2017;106:202-16.
[30] Wu Y-F, Xu X-S, Sun J-B, Jiang C. Analytical solution for the bond strength of externally bonded reinforcement. Compos Struct. 2012;94(11):3232-9.